THE JOURNAL OF BIOLOGICAL CHEMISTRY
Vol. 280, No. 28, Issue of July 15, pp. 26477–26482, 2005
Printed in U.S.A.

Engineering Conformational Destabilization into Mouse Apolipoprotein E

A MODEL FOR A UNIQUE PROPERTY OF HUMAN APOLIPOPROTEIN E4*

Received for publication, April 11, 2005, and in revised form, May 11, 2005
Published, JBC Papers in Press, May 11, 2005, DOI 10.1074/jbc.M503910200

Danny M. Hatters‡§, Clare A. Peters-Libeu‡§**, and Karl H. Weisgraber‡§¶‖**

From the ‡the Gladstone Institute of Neurological Disease, San Francisco, California 94158 and the §Cardiovascular Research Institute and ¶Department of Pathology, University of California, San Francisco, California 94143

Apolipoprotein (apo) E4 is a major risk factor for Alzheimer and cardiovascular diseases. ApoE4 differs from the two other common isoforms (apoE2 and apoE3) by its lower resistance to denaturation and greater propensity to form partially folded intermediates. As a first step to determine the importance of stability differences *in vivo*, we reengineered a partially humanized variant of the amino-terminal domain of mouse apoE (T61R mouse apoE) to acquire a destabilized conformation like that of apoE4. For this process, we determined the crystal structure of wild-type mouse apoE, which, like apoE4, forms a four-helix bundle, and identified two structural differences in the turn between helices 2 and 3 and in the middle of helix 3 as potentially destabilizing sites. Introducing mutations G83T and N113G at these sites destabilized the mouse apoE conformation. The mutant mouse apoE more rapidly remodeled phospholipid than T61R mouse apoE, which supports the hypothesis that a destabilized conformation promotes apoE4 lipid binding.

Apolipoprotein (apo)[1] E plays a central role in the transport and metabolic fate of lipids throughout the central nervous and cardiovascular systems (1–3). One of the common human isoforms, apoE4, is a major risk factor for cardiovascular and Alzheimer diseases. The other two common isoforms, apoE3 and apoE2, each correlate with a lowered risk, respectively, for Alzheimer disease (4–8). ApoE4 is also associated with poor outcome and recovery after neurological injury (9–11) and more rapid progression of multiple sclerosis and amyotrophic lateral sclerosis (12, 13).

The three isoforms are encoded by one gene and differ at one or two amino acid sequence positions. ApoE3 has a cysteine at position 112 and a arginine at 158, and apoE2 has cysteines and apoE4 has arginines at both positions (14). These sequence differences result in structural and biophysical properties that alter function and hence likely affect disease. In apoE4, the two modular domains interact in a unique manner known as domain interaction (15–17). Arg-112 in apoE4 causes the Arg-61 side chain to adopt a different conformation than it has in apoE2 and apoE3, allowing it to form a putative salt-bridge with Glu-255 in the carboxyl-terminal domain (16, 18).

The isoforms also differ in the conformational stability of the amino-terminal domains, which unfold independently from the carboxy-terminal domain and contain the isoform-specific sequence differences (19–22). The amino-terminal domain of apoE4 is the least resistant to chemical and thermal denaturation and that of apoE2 is most resistant (20, 22). The amino-terminal domain of apoE4 also most readily forms partially folded intermediates that have characteristics of a molten globule state (21).

Increasing evidence indicates that molten globules are common and mediate a wide variety of physiological processes, including translocation across membranes, increased affinity for membranes, binding to liposomes and phospholipids, protein trafficking, extracellular secretion, and cell cycle regulation (23). As one explanation for functional differences among the isoforms *in vivo*, we and others have suggested that partially folded intermediates provide apoE with greater conformational adaptability to bind to phospholipids (21, 24).

Previously, our laboratory introduced domain interaction into mouse apoE. Gene targeting was used to replace the threonine at the mouse equivalent of position 61 with an arginine (T61R), which resulted in an apoE4-like lipoprotein binding preference (25), a characteristic of domain interaction. However, unlike apoE4, T61R mouse apoE folds highly cooperatively and lacks apparent folding intermediates. To gain insight into how differences in isoform stability affect phenotype and disease, we sought to introduce into T61R mouse apoE the reduced folding stability characteristic of apoE4.

The objective here was to further humanize mouse apoE by replacing residues with those from apoE4 that destabilize the conformation. An empirical approach was taken to change the urea-denaturation curve of T61R mouse apoE to resemble that of apoE4. The crystal structure of the amino-terminal domain of wild-type mouse apoE was determined to identify potential structural differences between apoE4 and mouse apoE that might result in packing differences leading to differences in the urea denaturation curves.

MATERIALS AND METHODS

Protein Expression and Purification—cDNAs corresponding to the amino-terminal domains of human and mouse apoE were cloned into pET32a as an amino-terminal thioredoxin-his-tag fusion. Mutants were generated with the QuikChange mutagenesis kit (Stratagene), and DNA sequences were verified by DNA sequencing. The protein was expressed in *Escherichia coli* as described (26). After expression of a 6-liter culture, the cells were resuspended in 30 ml of 10 mM Tris, pH 7.4, 150 mM sodium chloride, 0.25 mM EDTA, 0.0005% sodium azide

* This work was supported by Grants P01 AG022074 and R01 AG020235 from the National Institutes of Health. The costs of publication of this article were defrayed in part by the payment of page charges. This article must therefore be hereby marked "*advertisement*" in accordance with 18 U.S.C. Section 1734 solely to indicate this fact.

The atomic coordinates and structure factors (code 1YA9) have been deposited in the Protein Data Bank, Research Collaboratory for Structural Bioinformatics, Rutgers University, New Brunswick, NJ (http://www.rcsb.org/).

‖ To whom correspondence should be addressed: Gladstone Institute of Neurological Disease, 1650 Owens St., San Francisco, CA 94158. Tel.: 415-734-2000; Fax: 415-355-0824; E-mail: kweisgraber@gladstone.ucsf.edu.

** Both authors contributed equally to this work.

[1] The abbreviations used are: apo, apolipoprotein; DMPC, dimyristoylphosphatidylcholine; Aβ, amyloid β.

(TBS). The cells were frozen, thawed, and lysed by sonication, and debris was removed by centrifugation at 15,000 × *g* for 20 min at 4 °C. Dimyristoylphosphatidylcholine (DMPC) powder (1.8 g) was added to the cell lysate, and the mixture was incubated overnight at 24 °C and dialyzed into 10 mM Tris, pH 8.0, with two buffer changes. The fusion protein was cleaved by adding 1 mg of bovine α-thrombin, and the mixture was incubated overnight at room temperature. The apoE·DMPC complexes were isolated by density gradient centrifugation: 0.3265 g/ml KBr was added to the lysate and overlaid with 1.48 M potassium bromide, 10 mM Tris, pH 7.4, in a Beckman/Coulter Quick-Seal tube; centrifugation was at 55,000 rpm for 12 h in a Beckman Ti60 rotor at 15 °C. The floated pellet was collected by slicing the tube. The DMPC·apoE fraction was dialyzed exhaustively against 0.1 M ammonium bicarbonate and lyophilized, delipidated, and purified by gel filtration as described (26). For crystallization, a final anion-exchange chromatography step involved DEAE-resin and a linear salt gradient. Protein concentrations were determined with the Lowry assay with bovine serum albumin as the mass standard.

Crystallization and X-ray Diffraction Data Collection—Crystals were grown by the hanging drop technique with 1.9 mg/ml of mouse apoE and 42.5% saturated sodium malonate, pH 7.2, 100 mM sodium acetate at pH 5.7. Diffraction data were collected at beam line 7-1 at the Stanford Synchrotron Radiation Laboratory. The data collection statistics are summarized in Table I. The space group was determined to be $P2_12_12_1$ and the unit cell is $a = 29.034$, $b = 49.233$, $c = 112.177$. Initial phases were obtained by using the molecular replacement program EPMR (27) and the structure of the amino-terminal domain of apoE4 as the starting model. To decrease model bias, RESOLVE (28) was used to refine the initial phases and build the preliminary model. CNS (29) and REFMAC (30) were used in subsequent refinement cycles.

Urea Denaturation Curves—A saturated urea solution was freshly deionized and filtered. The urea concentration was determined by measurement of the refractive index as described (31). Circular dichroism spectra were collected of the apoE 22-kDa fragment (0.5 mg/ml) in 0–8 M urea, 5 mM dithiothreitol, 20 mM sodium acetate, pH 4.0. Samples were preincubated overnight at 4 °C before the spectroscopic analysis, and data were collected at 24 °C using a 1-mm path length cuvette and an Applied Biophysics π-180 or Jasco J-720 CD spectrometer with a 1000-ms acquisition time. Ellipticity at 222 nm served as an indicator of secondary structure (which is predominately α-helical in the folded state), and data were adjusted to the fraction unfolded assuming that the protein is 100% unfolded in 8 M urea.

DMPC Turbidity-clearance Assays—Samples of the apoE 22-kDa fragment (1 mg/ml) were prepared in 1 mM Tris-carboxyethylphosphine and 20 mM sodium acetate, pH 4.0 (buffer A). DMPC was prepared at 5 mg/ml in buffer A, incubated at 42 °C for 20 min, and extruded through a 100-nm pore filter (Lipex pressure extruder). The resulting large unilamellar vesicles were diluted to 1 mg/ml in buffer A. The vesicles, protein samples, and spectrophotometer cuvette holding block were pre-equilibrated at 26 °C overnight. Samples of apoE or buffer A (200 μl) were mixed rapidly with vesicles (400 μl), and turbidity was monitored by absorbance at 325 nm for 20 min at 26 °C. Cuvettes were pre-equilibrated at 26 °C for 10 min before use.

RESULTS

Differences in the Urea Denaturation Curves of the Amino-terminal Domain of Mouse and Human ApoE—Urea denaturation studies showed that the amino-terminal domain of apoE4 has a lower apparent conformational stability than apoE3 and apoE2 and a greater tendency to form partially folded intermediates, as revealed by a less cooperative transition from the folded state to the unfolded state (21). The denaturation curve of T61R mouse apoE displayed greater cooperativity than apoE3 and apoE4 and unfolded at urea concentrations more similar to that at which apoE3 unfolds than apoE4 (Fig. 1). Wild-type mouse apoE had a denaturation curve similar to that of T61R mouse apoE (Fig. 1).

Structural Comparison of the Amino-terminal Domain of Mouse and Human ApoE—The crystal structure of the amino-terminal domain of wild-type mouse apoE was determined to a resolution of 2.1 Å and used to find clues for packing differences with apoE4 that may influence folding and stability. The x-ray diffraction data collection and refinement statistics are summarized in Table I.

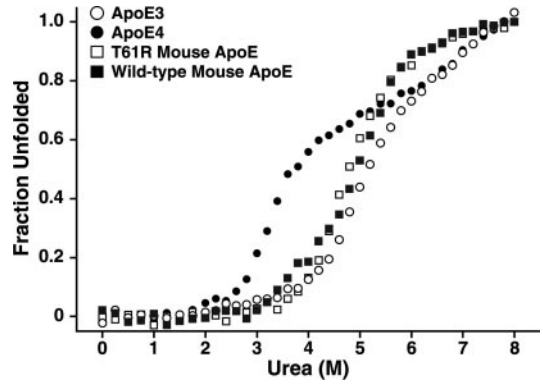

FIG. 1. **Urea denaturation curves of the amino-terminal domains of apoE isoforms.** Curves are derived from fractional change in CD ellipticity at a wavelength of 222 nm in 0–8 M urea. ApoE3 (○), apoE4 (●), wild-type mouse apoE (■), and T61R mouse apoE (□) are shown.

TABLE I
Data collection and refinement statistics

Data collection	
Resolution	20–2.09 Å (2.15–2.09 Å)
Observations	77746
Unique reflections	10097
R_{sym} [a,b]	0.03 (0.19)
$\langle I/\sigma(I)\rangle$	32.0 (6.75)
Completeness	0.97 (87)
Refinement	
Reflections used	9592
R-factor[c]	0.20 (0.20)
R_{free} [d]	0.27 (0.34)
Root mean square deviations	
Bond lengths (Å)	0.034
Bond angles (Å)	2294
PDB code	1YA9

[a] $R_{sym} = \Sigma_{ij} |I_{ij} - \langle I_i\rangle| / \Sigma \langle I_i\rangle$, where I_{ij} is the intensity of an individual observation of the i^{th} reflection, and $\langle I_i\rangle$ is the average intensity of the ith reflection.

[b] The values for the highest shell of reflections (2.13–2.09 Å) are shown in parentheses.

[c] R-factor $= \Sigma_i |Fc_i - Fo_i| / \Sigma \langle Fo_i\rangle$, where Fc_i is the structure factor calculated from the model, and Fo_i is the observed structure factor for the ith reflection. This statistic is calculated from the set of reflections used during refinement (95% of the total reflections).

[d] R_{free} is the R-factor calculated from a set of randomly selected reflections (5% of the unique reflections) not used in refinement.

Excluding the eight additional amino-terminal residues of human apoE, the amino-terminal domains of mouse apoE and apoE4 differ at 35 sequence positions, corresponding to 81% sequence identity (Fig. 2). The overall fold of the amino-terminal domain of wild-type mouse apoE is similar to apoE4 (Fig. 3 (32)). Except for residues 9–11, 166–172, and 186–191, the residues of the amino-terminal domain of mouse apoE are clearly visible in the final electron density map.

Although the amino-terminal domain of mouse apoE, like that of apoE4, forms a four-helix bundle, there are structural differences. Alignment of the mouse and human structures along helices 1 and 2 shows that relative to apoE4 helices 3 and 4 (of the amino-terminal domain) of mouse apoE are shifted in a direction roughly parallel to the helical axis of helix 3. In addition, helices 1, 2, and 4 are longer in mouse apoE than in apoE4. A crystal contact at residue 20 in mouse apoE likely stabilizes the extension of helix 1; in apoE4 no such contact occurs. A crystal contact at residue 126 of mouse apoE, which is not seen in apoE4, likely influences the structure of the loop between helices 3 and 4 (residues 120–130).

Two Structural Differences at Positions 83 and 113 Are Mediated by Sequence Differences—After exclusion of the crystal contact sites, two key structural differences result from the

sequence differences. The loop between helices 2 and 3 (residues 81–86) forms a tight turn in mouse apoE but is more extended and relaxed in all crystal structures of human apoE (33). This difference reflects the *cis* conformation of Gly-83 in mouse apoE, which cannot be sterically accommodated by Thr-83 in apoE4 (Fig. 4*A*). In mouse apoE, helix 2 has one more helical turn than apoE4, and the dipoles of helices 2 and 3 are less parallel (Fig. 4*B*).

The other major difference is at residue 113, where mouse apoE contains asparagine, and apoE4 contains glycine (Fig. 4, *B* and *C*). Asn-113 in mouse apoE lies in a straight portion of helix 3, but the Gly-113 in apoE4 lies at a pronounced kink and cannot form the same hydrogen bond with Arg-112 that is formed by Asn-113 in mouse apoE (Fig. 4*C*). The result is a reduced local hydrogen bond network (Fig. 4*C* and Table II). In addition, because glycines have high configurational entropy, localized flexibility in the middle of helix 3 caused by Gly-113 may account for the lower stability and greater propensity of apoE4 to form partially folded intermediates. The net effects of both sequence differences at positions 83 and 113 are a greater stabilization of helix 3 and a more parallel alignment of the dipoles of helices 2 and 3 in mouse apoE than in apoE4 (Fig. 4*B*). Thus, these data suggest that these two sequence differences contribute to the differences in the human and mouse urea denaturation curves.

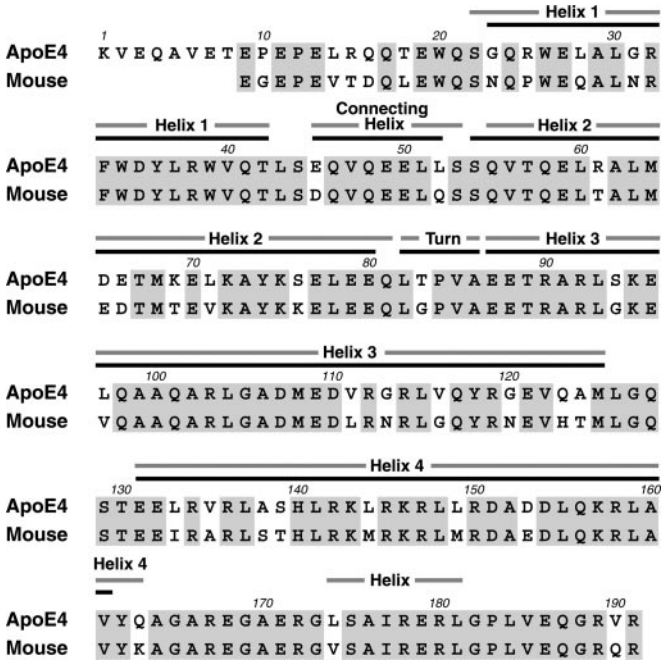

FIG. 2. **Sequence alignment of the amino-terminal domains of mouse apoE and apoE4.** The numbering system for mouse apoE is standardized to the apoE4 sequence (apoE4 has eight additional amino-terminal residues). Identical residues are highlighted in *gray*. Major structural elements are noted above sequence (apoE4, *black bars*; mouse apoE, *gray bars*).

Introducing ApoE4 Residues at Positions 83 and 113 Destabilizes T61R Mouse ApoE—Thr-83 and Gly-113 of apoE4 were introduced into T61R mouse apoE with the prediction that they would destabilize the global conformation. The urea denaturation curves showed that the mutants unfolded in urea more readily than T61R mouse apoE and that the mutations had additive effects in destabilizing the conformation (Fig. 5*A*). The triple mutant mouse apoE (T61R, G83T, N113G) and apoE4 displayed similar denaturation curves in the range of 0–4.5 M urea, suggesting that the mutations at position 83 and 113 account for the largest effects on the differences in stability between T61R mouse E and apoE4 (Fig. 5*B*).

Seven more mutants were made to probe the influence of other structural differences. We introduced apoE4 residues at Q52L and/or H123Q, which occur at sites of crystal contacts, or apoE4 residues M114L and M149L together, which correlate with differences in the packing of the core into T61R mouse apoE. These mutations had only marginal effects on the urea denaturation curves (data not shown). Three other mutants were made with the T61R, G83T, N113G backbone that introduced nonconservative sequence differences, all with minimal effects on stability. Introducing the apoE4 residues G94S and N120G or the group of residues N23G, G94S, N120G, P25R, G116V, and Q28L slightly reduced folding cooperativity and stability (Fig. 5*B*). Introduction of all apoE4 residues (*i.e.* the apoE4 sequence without the first eight amino acids) yielded a urea denaturation curve similar to that of apoE4 (Fig. 5*B*). This suggests that the additional eight residues in apoE4 play a minor role in stability. In contrast to mutations G83T and N113G, this collection of seven group mutations have minor effects on the urea denaturation curve.

Destabilizing Mutations, G83T and N113G, Increase Lipid Binding of T61R Mouse ApoE—Because stability differences in the amino-terminal domains of human apoE isoforms correlate inversely with lipid binding (21, 34), we examined the lipid binding of destabilized mouse apoE. Lipid binding was assessed with a standard apolipoprotein lipid binding assay that examines the ability of apoE to remodel large unilamellar vesicles of DMPC (35). Upon binding to DMPC vesicles, apoE forms smaller apoE·DMPC particles, thereby decreasing the turbidity of the solution (36). Of the human isoforms, apoE4 clears the turbidity fastest, followed by apoE3 and apoE2 (21). The amino-terminal domain of apoE4 cleared the turbidity in an exponential decay-like manner and much faster than T61R mouse apoE (Fig. 6). The

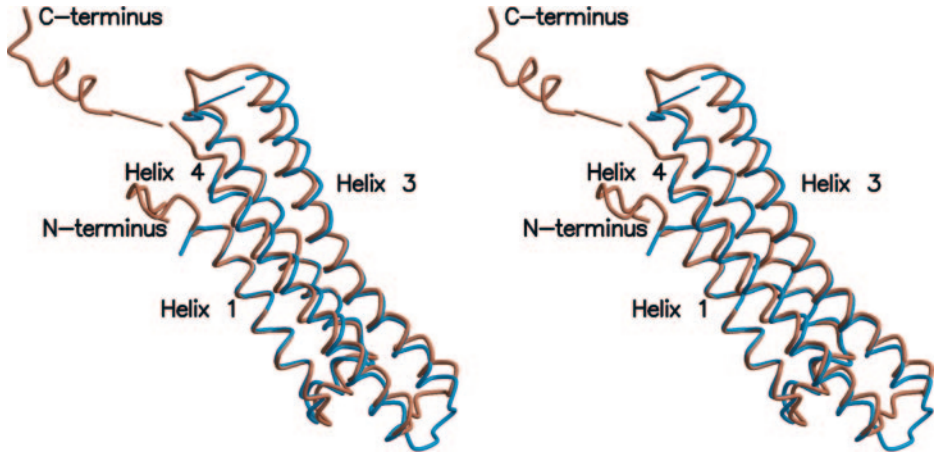

FIG. 3. **Stereo image of an overlay of the crystal structures of the amino-terminal domain of mouse apoE and apoE4.** The α-carbon traces of apoE4 (*blue*) and mouse apoE (*orange*) are shown. The backbone deviation between helices 2 and 3 in each crystal form is 0.5–1.0 Å.

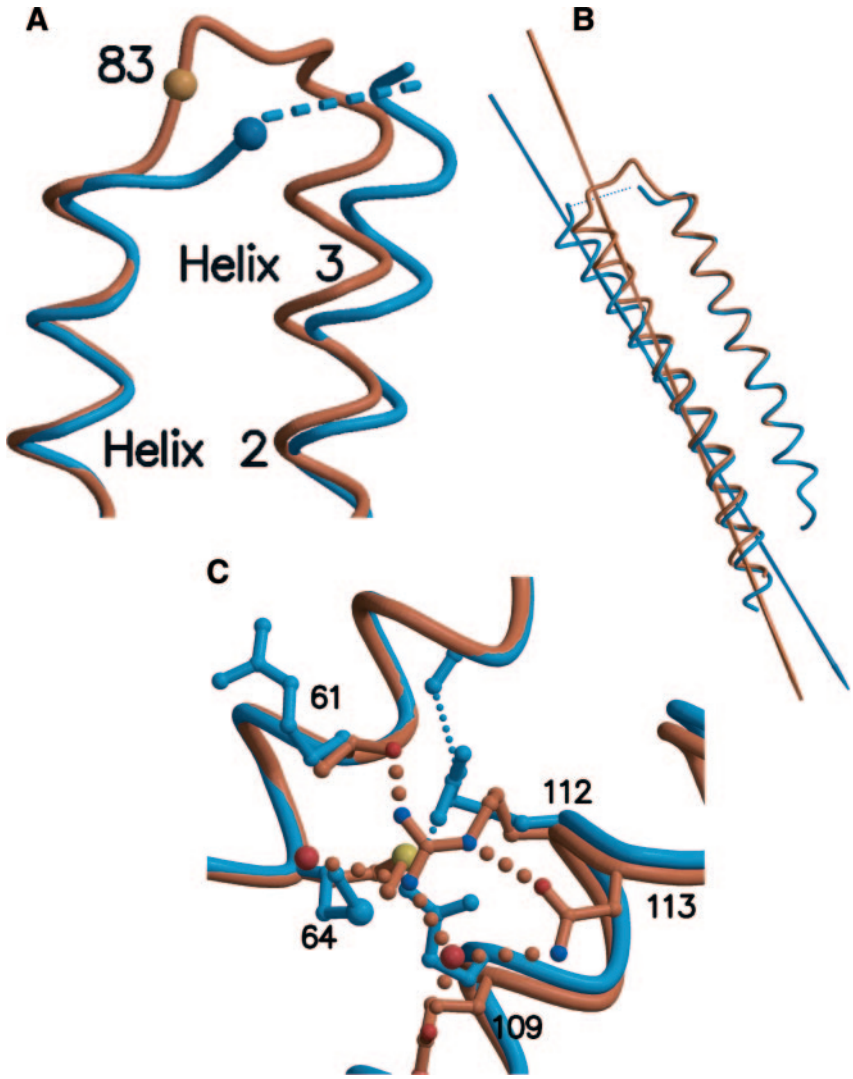

FIG. 4. **Key structural differences between mouse apoE and apoE4 amino-terminal domains.** *A*, differences in the α-carbon trace overlay of mouse apoE (*yellow*) and apoE4 (*cyan*) at the loop between helices 2 and 3 are influenced by residue 83. *B*, differences in the helical dipoles of helix 3 of mouse apoE (*yellow*) and apoE4 (cyan) (only helices 2 and 3 are shown). *C*, differences in the hydrogen bond network of mouse apoE (*yellow*) and apoE4 (*cyan*) influenced by residue 113.

TABLE II
Potential hydrogen bonds in mouse apoE and human apoE4 near 112

		Mouse		ApoE4	
		Distance	Residue	Distance	Residue
		Å		Å	
Arg-112	NH_1	3.53	W2 OH	2.94	109 OE1
Arg-112	NH_1	3.68	W1 OH		
Arg-112	NH_2	2.36	T61 OG1	3.29	W 38 OH_2[a]
Arg-112	NE	3.35	N113 OD1	3.23	T 57 O
Arg-113	ND2	3.44	W1 OH		

[a] Not shown in picture.

destabilizing mutations, G83T and N113G, each cleared faster than T61R mouse apoE, and both mutations together further increased the clearance rate (Fig. 6).

DISCUSSION

Our objective in this study was to introduce instability into the mouse apoE mutant (T61R) that displays domain interaction, making it more apoE4-like. Based on a comparison of the x-ray crystal structures of the amino-terminal domains of human apoE4 and wild-type mouse apoE, we identified two potential structural differences in the loop connecting helices 2 and 3 (position 83) and the middle of helix 3 (position 113) that likely would affect stability. Although there are several other differences between human and mouse apoE, we found that introduction of human residues G83T and N113G into the loop between helices 2 and 3 and the middle of helix 3 were all that was required to mimic the unfolding behavior of apoE4 (Fig. 7). The destabilized T61R mouse apoE has increased lipid binding properties, demonstrating an analogous functional switch from apoE3-like to apoE4-like. It is interesting that stability of the apoE isoforms (apoE4 < apoE3 < apoE2) parallels the relative susceptibility of carriers of these isoforms to Alzheimer disease.

This new model of apoE4 will be useful for testing and exploring the cooperative or additive effects of both domain interaction and a lower stability. Furthermore, because T61R introduces domain interaction into wild-type mouse apoE, a mouse model specific for apoE4-reduced stability but without domain interaction can be made by the mutation E255A (16).

For several other proteins, mutations or conditions that destabilize the native conformation also facilitate the formation of aggregates with properties of amyloid fibrils, which consist of an ordered polymer of β-strands (37–39). Thus, the destabilization of the compactly folded state of apoE, although advantageous for lipid binding, may predispose misfolding into amyloid fibrils. This could provide a basis for amyloid formation because amyloid plaques in brains of Alzheimer patients show apoE immunoreactivity (40, 41). The apoE isoforms differ in their ability to promote amyloid formation by Aβ. *In vitro*, co-incubation of purified apoE with Aβ, promotes Aβ fibrillization, and the fibrils are coated with apoE (42). ApoE4 facilitates the formation of a more extensive matrix of Aβ fibrils than does apoE3, as assessed by electron microscopy (42, 43).

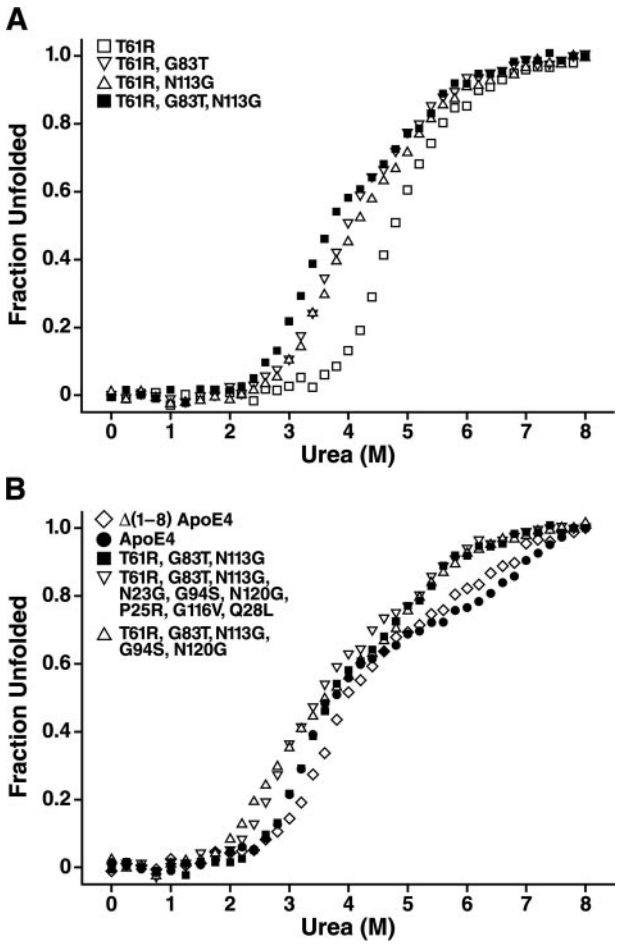

FIG. 5. **Effect of mutations on the urea denaturation curves of T61R mouse apoE compared with apoE4.** *A*, the amino-terminal domain of T61R mouse apoE (□), T61R, G83T mouse apoE (▽), T61R, N113G mouse apoE (△), and the triple mutant T61R, G83T, N113G mouse apoE (■) are shown. *B*, the amino-terminal domains of completely humanized mouse apoE (Δ(1–8) apoE4, ◇), apoE4 (●), the triple mutant T61R,G83T,N113G mouse apoE (■), the multiple mutant T61R,G83T,N113G,N23G,G94S,N120G,P25R,G116V,Q28L mouse apoE (▽), and multiple mutant T61R,G83T,N113G,G94S,N120G mouse apoE (△) are shown.

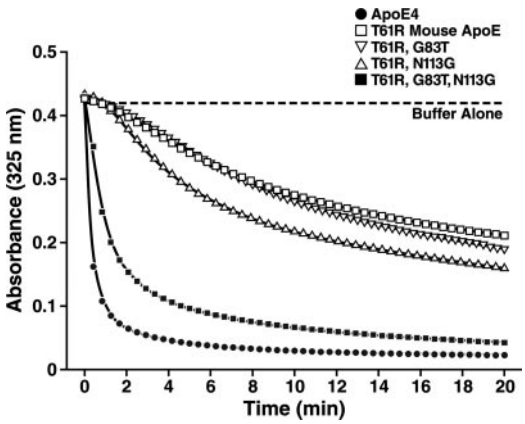

FIG. 6. **Turbidity clearance assay of apoE amino-terminal domains.** Change in absorbance was followed after the addition of apoE to DMPC multilamellar vesicles. Data shown are apoE4 (●), the single mutant T61R mouse apoE (□), the double mutants T61R,G83T mouse apoE (▽) and T61R,N113G mouse apoE (△), the triple mutant T61R,G83T,N113G mouse apoE (■), and buffer alone (*dashed line*).

In vivo, the gene dosage of apoE4 in Alzheimer patients correlates with deposition of amyloid (44). In mouse models of Alzheimer disease (*i.e.* mice expressing human amyloid precursor protein and human apoE isoforms) apoE4 is more effective in promoting the deposition of Aβ than apoE3 (45–49). Furthermore, in apoE knock-out mice expressing human apoE isoforms, apoE4 drives the nucleation and aggregation of immunopositive Aβ deposits to a greater extent than apoE3 (50). Differences in the co-aggregation of the apoE isoforms with Aβ may provide a mechanism for the acceleration of Aβ nucleation, polymerization, and plaque formation.

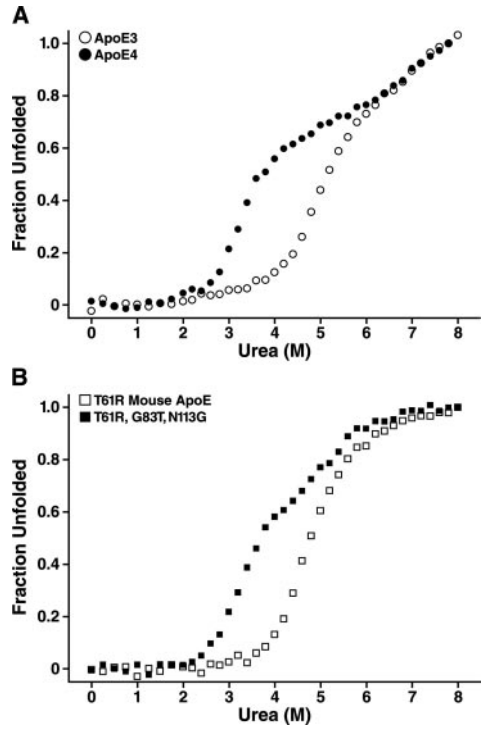

FIG. 7. **Urea denaturation curves of the amino-terminal domains of human and partially humanized mouse apoE mutants.** *A*, ApoE3 (○) and apoE4 (●) are shown. *B*, T61R mouse apoE (□) and T61R,G83T,N113G mouse apoE (■) are shown.

The enhanced lipid remodeling properties of a destabilized apoE could also influence cellular functioning and result in pathologic effects. ApoE4, but not apoE3, potentiates Aβ-induced lysosomal leakage in cultured neuronal cells, suggesting that apoE4 destabilizes lysosomal membrane integrity cooperatively with Aβ (51). Our results support the hypothesis that the greater phospholipid binding ability of destabilized variants apoE accounts for greater permeabilization of phospholipid membranes.

A mouse model of apoE4 conformational stability will be a valuable tool for studying potential mechanisms. In addition, this system will provide a unique model for exploring the role of conformational stability in protein function and pathology directly *in vivo*.

Acknowledgments—We thank Jon Menke, Maryam Tabar, Yvonne Newhouse, and Earl Rutenber for their technical assistance; Stephen Ordway and Gary Howard for editorial assistance; John Carroll, Jack Hull, Stephen Gonzales, and Chris Goodfellow for graphics assistance; and Karina Fantillo for manuscript preparation.

REFERENCES

1. Boyles, J. K., Pitas, R. E., Wilson, E., Mahley, R. W., and Taylor, J. M. (1985) *J. Clin. Investig.* **76,** 1501–1513
2. Pitas, R. E., Boyles, J. K., Lee, S. H., Hui, D., and Weisgraber, K. H. (1987) *J. Biol. Chem.* **262,** 14352–14360
3. Mahley, R. W. (1988) *Science* **240,** 622–630
4. Saunders, A. M., Strittmatter, W. J., Schmechel, D., St George-Hyslop, P. H., Pericak-Vance, M. A., Joo, S. H., Rosi, B. L., Gusella, J. F., Crapper-MacLachlan, D. R., Alberts, M. J., Hulette, C., Crain, B., Goldgaber, D., and Roses, A. D. (1993) *Neurology* **43,** 1467–1472
5. Corder, E. H., Saunders, A. M., Strittmatter, W. J., Schmechel, D. E., Gaskell, P. C., Small, G. W., Roses, A. D., Haines, J. L., and Pericak-Vance, M. A.

(1993) *Science* **261,** 921–923
6. Strittmatter, W. J., and Roses, A. D. (1995) *Proc. Natl. Acad. Sci. U. S. A.* **92,** 4725–4727
7. Saunders, A. M., Schmader, K., Breitner, J. C. S., Benson, M. D., Brown, W. T., Goldfarb, L., Goldgaber, D., Manwaring, M. G., Szymanski, M. H., McCown, N., Dole, K. C., Schmechel, D. E., Strittmatter, W. J., Pericak-Vance, M. A., and Roses, A. D. (1993) *Lancet* **342,** 710–711
8. Nathan, B. P., Bellosta, S., Sanan, D. A., Weisgraber, K. H., Mahley, R. W., and Pitas, R. E. (1994) *Science* **264,** 850–852
9. Mayeux, R., Ottman, R., Maestre, G., Ngai, C., Tang, M.-X., Ginsberg, H., Chun, M., Tycko, B., and Shelanski, M. (1995) *Neurology* **45,** 555–557
10. Slooter, A. J. C., Tang, M.-X., van Duijn, C. M., Stern, Y., Ott, A., Bell, K., Breteler, M. M. B., Van Broeckhoven, C., Tatemichi, T. K., Tycko, B., Hofman, A., and Mayeux, R. (1997) *J. Am. Med. Assoc.* **277,** 818–821
11. Teasdale, G. M., Nicoll, J. A. R., Murray, G., and Fiddes, M. (1997) *Lancet* **350,** 1069–1071
12. Fazekas, F., Strasser-Fuchs, S., Schmidt, H., Enzinger, C., Ropele, S., Lechner, A., Flooh, E., Schmidt, R., and Hartung, H.-P. (2000) *J. Neurol. Neurosurg. Psychiatry* **69,** 25–28
13. Drory, V. E., Birnbaum, M., Korczyn, A. D., and Chapman, J. (2001) *J. Neurol. Sci.* **190,** 17–20
14. Weisgraber, K. H., Rall, S. C., Jr., and Mahley, R. W. (1981) *J. Biol. Chem.* **256,** 9077–9083
15. Dong, L.-M., Wilson, C., Wardell, M. R., Simmons, T., Mahley, R. W., Weisgraber, K. H., and Agard, D. A. (1994) *J. Biol. Chem.* **269,** 22358–22365
16. Dong, L.-M., and Weisgraber, K. H. (1996) *J. Biol. Chem.* **271,** 19053–19057
17. Xu, Q., Brecht, W. J., Weisgraber, K. H., Mahley, R. W., and Huang, Y. (2004) *J. Biol. Chem.* **279,** 25511–25516
18. Weisgraber, K. H., and Mahley, R. W. (1996) *FASEB J.* **10,** 1485–1494
19. Wetterau, J. R., Aggerbeck, L. P., Rall, S. C., Jr., and Weisgraber, K. H. (1988) *J. Biol. Chem.* **263,** 6240–6248
20. Morrow, J. A., Segall, M. L., Lund-Katz, S., Phillips, M. C., Knapp, M., Rupp, B., and Weisgraber, K. H. (2000) *Biochemistry* **39,** 11657–11666
21. Morrow, J. A., Hatters, D. M., Lu, B., Höchtl, P., Oberg, K. A., Rupp, B., and Weisgraber, K. H. (2002) *J. Biol. Chem.* **277,** 50380–50385
22. Acharya, P., Segall, M. L., Zaiou, M., Morrow, J., Weisgraber, K. H., Phillips, M. C., Lund-Katz, S., and Snow, J. (2002) *Biochim. Biophys. Acta* **1584,** 9–19
23. Ptitsyn, O. B. (1995) *Adv. Protein Chem.* **47,** 83–229
24. Weers, P. M. M., Narayanaswami, V., Choy, N., Luty, R., Hicks, L., Kay, C. M., and Ryan, R. O. (2003) *Biophys. Chem.* **100,** 481–492
25. Raffaï, R. L., Dong, L.-M., Farese, R. V., Jr., and Weisgraber, K. H. (2001) *Proc. Natl. Acad. Sci. U. S. A.* **98,** 11587–11591
26. Morrow, J. A., Arnold, K. S., and Weisgraber, K. H. (1999) *Protein Expression Purif.* **16,** 224–230
27. Kissinger, C. R., Gehlhaar, D. K., and Fogel, D. B. (1999) *Acta Crystallogr. Sect. D* **55,** 484–491
28. Terwilliger, T. C., and Berendzen, J. (1999) *Acta Crystallogr. Sect. D* **55,** 849–861
29. Brünger, A. T., Adams, P. D., Clore, G. M., DeLano, W. L., Gros, P., Grosse-Kunstleve, R. W., Jiang, J.-S., Kuszewski, J., Nilges, M., Pannu, N. S., Read, R. J., Rice, L. M., Simonson, T., and Warren, G. L. (1998) *Acta Crystallogr. Sect. D* **54,** 905–921
30. Murshudov, G. N., Vagin, A. A., and Dodson, E. J. (1997) *Acta Crystallogr. Sect. D* **53,** 240–255
31. Pace, C. N. (1986) *Methods Enzymol.* **131,** 266–280
32. Wilson, C., Wardell, M. R., Weisgraber, K. H., Mahley, R. W., and Agard, D. A. (1991) *Science* **252,** 1817–1822
33. Segelke, B. W., Forstner, M., Knapp, M., Trakhanov, S. D., Parkin, S., Newhouse, Y. M., Bellamy, H. D., Weisgraber, K. H., and Rupp, B. (2000) *Protein Sci.* **9,** 886–897
34. Segall, M. L., Dhanasekaran, P., Baldwin, F., Anantharamaiah, G. M., Weisgraber, K. H., Phillips, M. C., and Lund-Katz, S. (2002) *J. Lipid Res.* **43,** 1688–1700
35. Pownall, H. J., Massey, J. B., Kusserow, S. K., and Gotto, A. M., Jr. (1978) *Biochemistry* **17,** 1183–1188
36. Saito, H., Dhanasekaran, P., Baldwin, F., Weisgraber, K. H., Phillips, M. C., and Lund-Katz, S. (2003) *J. Biol. Chem.* **278,** 40723–40729
37. Booth, D. R., Sunde, M., Bellotti, V., Robinson, C. V., Hutchinson, W. L., Fraser, P. E., Hawkins, P. N., Dobson, C. M., Radford, S. E., Blake, C. C. F., and Pepys, M. B. (1997) *Nature* **385,** 787–793
38. Nettleton, E. J., Sunde, M., Lai, Z., Kelly, J. W., Dobson, C. M., and Robinson, C. V. (1998) *J. Mol. Biol.* **281,** 553–564
39. Fändrich, M., Fletcher, M. A., and Dobson, C. M. (2001) *Nature* **410,** 165–166
40. Namba, Y., Tomonaga, M., Kawasaki, H., Otomo, E., and Ikeda, K. (1991) *Brain Res.* **541,** 163–166
41. Wisniewski, T., Lalowski, M., Golabek, A., Vogel, T., and Frangione, B. (1995) *Lancet* **345,** 956–958
42. Sanan, D. A., Weisgraber, K. H., Russell, S. J., Mahley, R. W., Huang, D., Saunders, A., Schmechel, D., Wisniewski, T., Frangione, B., Roses, A. D., and Strittmatter, W. J. (1994) *J. Clin. Investig.* **94,** 860–869
43. Ma, J., Yee, A., Brewer, H. B., Jr., Das, S., and Potter, H. (1994) *Nature* **372,** 92–94
44. Schmechel, D. E., Saunders, A. M., Strittmatter, W. J., Crain, B. J., Hulette, C. M., Joo, S. H., Pericak-Vance, M. A., Goldgaber, D., and Roses, A. D. (1993) *Proc. Natl. Acad. Sci. U. S. A.* **90,** 9649–9653
45. Bales, K. R., Verina, T., Dodel, R. C., Du, Y., Altstiel, L., Bender, M., Hyslop, P., Johnstone, E. M., Little, S. P., Cummins, D. J., Piccardo, P., Ghetti, B., and Paul, S. M. (1997) *Nat. Genet.* **17,** 263–264
46. Holtzman, D. M., Bales, K. R., Wu, S., Bhat, P., Parsadanian, M., Fagan, A. M., Chang, L. K., Sun, Y., and Paul, S. M. (1999) *J. Clin. Investig.* **103,** 15–21
47. Holtzman, D. M., Bales, K. R., Tenkova, T., Fagan, A. M., Parsadanian, M., Sartorius, L. J., Mackey, B., Olney, J., McKeel, D., Wozniak, D., and Paul, S. M. (2000) *Proc. Natl. Acad. Sci. U. S. A.* **97,** 2892–2897
48. Brendza, R. P., Bales, K. R., Paul, S. M., and Holtzman, D. M. (2002) *Mol. Psychiatry* **7,** 132–135
49. Buttini, M., Yu, G.-Q., Shockley, K., Huang, Y., Jones, B., Masliah, E., Mallory, M., Yeo, T., Longo, F. M., and Mucke, L. (2002) *J. Neurosci.* **22,** 10539–10548
50. Dolev, I., and Michaelson, D. M. (2004) *Proc. Natl. Acad. Sci. U. S. A.* **101,** 13909–13914
51. Ji, Z.-S., Miranda, R. D., Newhouse, Y. M., Weisgraber, K. H., Huang, Y., and Mahley, R. W. (2002) *J. Biol. Chem.* **277,** 21821–21828